Journal of Power Sources 221 (2013) 1–5

Contents lists available at SciVerse ScienceDirect

Journal of Power Sources

journal homepage: www.elsevier.com/locate/jpowsour

Short communication

A direct glucose alkaline fuel cell using MnO_2–carbon nanocomposite supported gold catalyst for anode glucose oxidation

Lei Li [a], Keith Scott [b], Eileen Hao Yu [b,*]

[a] School of Chemistry and Chemical Engineering, Shanghai Jiao Tong University, Shanghai 200240, China
[b] School of Chemical Engineering and Advanced Materials, Newcastle University, Newcastle upon Tyne NE1 7RU, United Kingdom

HIGHLIGHTS

- First study of using Au/MnO_2–C nanocomposite as the anode catalyst for direct glucose alkaline fuel cells (DGAFCs).
- Higher activity than Pt/C and Au/C from Au/MnO_2–C but with less noble metal.
- A promising approach to enhance activity of glucose oxidation catalysts with lower cost.

ARTICLE INFO

Article history:
Received 10 May 2012
Received in revised form
2 August 2012
Accepted 8 August 2012
Available online 16 August 2012

Keywords:
Glucose oxidation
Alkaline fuel cell
MnO_2/carbon
Gold
Nanocomposite

ABSTRACT

Gold nanoparticles supported on MnO_2–carbon nanocomposite (Au/MnO_2–C) are synthesised as the catalyst for the anodic oxidation of glucose for use in a direct glucose alkaline fuel cell (DGAFC). Characterisation of the catalyst is carried out using physical and electrochemical methods. It is observed that gold nanoparticles are uniformly dispersed onto the MnO_2–carbon nanocomposite support. Cyclic voltammetry shows that the prepared Au/MnO_2–carbon catalysts exhibit higher electro–catalytic activity for glucose oxidation than that of commercial Pt/C and Au/C catalysts. A maximum power density, at 30 °C, of 1.1 mW cm^{-2} is obtained using an Au/MnO_2–C anode catalyst in DGAFC, which is higher than that of the commercial Au/C catalyst. The enhanced activity is attributed to a catalytic effect of MnO_2 towards glucose oxidation. MnO_2–C nanocomposite is a promising approach for reducing noble metal catalyst loading in addition to improving the catalytic activity of gold catalyst for glucose oxidation.

1. Introduction

Glucose is produced in abundance from both naturally occurring plants and industrial processes. Glucose and its derivates represent more than 50% of the weight in flora. Wastewater from paper and food industries can contain high amounts of glucose. The energy density of glucose on complete oxidation to CO_2 via 24-electron transfer is 2.87×10^6 J mol^{-1} [1,2]. Compared to alcohol fuels, such as methanol and ethanol, which have been used widely in direct oxidation fuel cells (DOFCs), glucose is nontoxic, non-flammable, odourless and renewable. These properties make glucose an attractive fuel for various applications, particularly for portable electronic devices [3–5]. Despite these advantages, fuel cells using glucose are still far from achieving practical applications. Poor glucose oxidation at the anode is one of the major challenges in the development of direct glucose fuel cells. Enzymes, such as glucose oxidase [6] and glucose dehydrogenase [7] are efficient catalysts for glucose oxidation, and have been used to develop enzymatic glucose-air fuel cells. A maximum power density of 1.45 mW cm^{-2} is reported [7]. However, poor enzyme stability which results in a short operating life time of such system is a major limitation. The high cost of enzymes under current production conditions makes the system uneconomic to scale up to an industrial application.

Direct glucose alkaline fuel cells (DGAFCs) that directly produce electricity from glucose seem a potential choice for broader applications. However glucose is a very stable compound, which makes it difficult to be oxidised electrochemically. Studies on DGAFC have been reported recently [2,8,9]. Currently, only in a biological system, the complete glucose oxidation, generating twenty four electrons, can be achieved. In chemical oxidation, however, glucose oxidation will mainly go through a process generating two electrons [2,10]. The power density performance of DGAFCs, is much lower than that of alcohol fuel cells. The reported power densities are around two orders of magnitude lower than that of a typical

* Corresponding author. Fax: +44 1912225292.
E-mail address: eileen.yu@ncl.ac.uk (E.H. Yu).

0378-7753/$ – see front matter © 2012 Elsevier B.V. All rights reserved.
http://dx.doi.org/10.1016/j.jpowsour.2012.08.021

proton exchange membrane fuel cell (PEMFC). The highest power density reported to date for a DGAFC is 38 mW cm^{-2} [8] using an anion exchange membrane (AEM) in 7.0 M KOH at 60 °C with pure oxygen at the cathode. Basu and Basu report a maximum power density of 1.6 mW cm^{-2} mg^{-1} Pt with Pt/Au oxidation catalyst under relatively mild condition, i.e. ambient temperature, and aqueous 1 M KOH electrolyte [11].

Generally it is important to develop low cost catalysts with high catalytic activity towards glucose oxidation. Noble metal based catalyst, such as, Pt [2], nanoporous gold (NPG) [12,13], bi-metallic catalysts of Pd–Pt [14,15], Ag–Au [16–18], Pt–Ru [1], Pt–Au [11,19,20], Pt–Bi [11] and Pd–Ni [8], as well as Pt–Pd–Au ternary catalysts [20] are reported for glucose oxidation in alkaline media. Gold and some binary alloys of gold are promising active catalysts for glucose oxidation. Manganese oxide (MnO_2) is also reported as a glucose oxidation catalyst for use in glucose sensors [21], and exhibits reasonable activity for oxidation of other carbohydrates, such as fructose [22]. Improved electrocatalytic activity for glucose oxidation is obtained with an Au coated MnO_2 film in a glucose sensor, and the improvement of activity is attributed to catalytic effects of MnO_2 and gold [23]. The low cost of MnO_2 could provide the possibility of reducing noble metal content for glucose oxidation catalysts.

In this study, the synthesis of a gold nanoparticle catalyst supported on a manganese oxide–carbon nanocomposite substrate (Au/MnO_2–C) is reported for the first time for use in DGAFCs. Physical characterisation of the catalyst is conducted using scanning electron microscope (SEM), transmission electron microscope (TEM) and X-ray diffraction (XRD). Electrocatalytic activity of the catalyst for glucose oxidation is examined using cyclic voltammetry (CV) and in fuel cell polarisations in alkaline medium at 30 °C.

2. Experimental

2.1. Preparation of MnO_2–C nanocomposite support

$MnSO_4$ (Sigma Aldrich) and Vulcan XC72 carbon (Akzo Nobel) are employed to prepare MnO_2–C catalyst support. 100 ml of de-ionised water is used as solvent to disperse the XC72 carbon (0.6 g) and $MnSO_4$ (0.12 g, 10 mmol) at 90 °C for 1 h, 0.16 g (10 mmol) of $KMnO_4$ (Sigma Aldrich) is added to the carbon–$MnSO_4$ mixture for a further 1 h to carry out the following reaction under stirring:

$$2KMnO_4 + 3MnSO_4 + 2H_2O \rightarrow 5MnO_2 + 2H_2SO_4 + K_2SO_4 \quad (1)$$

After reaction, the mixture is centrifuged for 3 min at 5000 rpm to separate the MnO_2–C particles from the solvent. The MnO_2–C particles are washed with de-ionised water and then with ethanol to minimise impurities. The MnO_2–C particles were dried in an oven at 100 °C for 10 h before deposition of Au.

2.2. Preparation of Au/MnO_2–C catalyst

Gold nanoparticles supported on MnO_2–C support is prepared by impregnation of chloroauric acid (Sigma Aldrich) aqueous solution with MnO_2–C nanocomposite followed by a chemical reduction with sodium borohydride ($NaBH_4$, Sigma Aldrich). 48 mg of MnO_2–C is ultrasonicated in 50 ml of de-ionised water for 1 h and then stirred for a further 2 h. 1.2 ml of 1 wt% chloroauric acid solution was added to the solution under stirring for 10 min. 2 cm^3 (ml) of 0.1 M $NaBH_4$ in 1 M NaOH solution is added slowly and the reaction is continued for 12 h at room temperature. After the reaction, the mixture is centrifuged and the particles are washed thoroughly and dried at 80 °C for 3 h. The Au content in the catalysts is 20 wt%.

2.3. Physical characterisation of Au/MnO_2–C catalyst

Scanning electron microscopy (SEM, JEM-100CX) and transmission electron microscopy (TEM, JEOL S-520) are used to determine the surface morphology and the particle size of the catalyst. X-ray diffraction (XRD) is carried out on D/max-2200/PC X-Ray Diffractometer with an area detector using a Cu Kα radiation source ($\lambda = 1.54056$ Å) to study the crystal structure of the catalyst.

2.4. Electrochemical characterisation and fuel cell tests

Cyclic voltammetry (CV) is carried out with Autolab PGSTAT 302 (Eco Chemie, the Netherlands) using a three-electrode cell with Autolab Model 616 rotating disk electrode (RDE). A platinum foil is used as the counter electrode, and an Hg/HgO (0.140 V vs NHE) electrode is used as the reference electrode, respectively. The potentials reported in this work are reported against the Hg/HgO reference electrode unless otherwise stated. The working electrode on RDE system is a glassy carbon disk (3 mm o.d) coated with different catalysts. The catalyst ink is prepared by mixing 21.2 mg 20 wt% Au/MnO_2–C into 200 μl water, 30 μl 5 wt% Nafion solution (Sigma Aldrich) and 2.5 ml ethanol in an ultrasonic water bath for 40 min. 3 μl of the catalyst ink is pipetted on the glassy carbon electrode to give a loading of ca. 0.086 mg cm^{-2}. 0.5 M glucose in 1 M NaOH aqueous solution is used for glucose oxidation measurements. High-purity N_2 is sparged into the electrolyte during the experiments.

The fuel cell performance was evaluated in a small single cell similar to that reported by Basu et al. [1,11,20]. The anode catalyst is the prepared Au/MnO_2–C, and the cathode catalyst was activated charcoal (Qualigen Fine Chemicals). The area of each electrode is 4 cm^2. The cathode is a self-breathing passive air cathode. The catalyst loading in each electrode is 3 mg cm^{-2}. No membrane is used. The catalyst slurry is prepared by dispersing the required amount of catalyst powder in a few drops of an equal volume mixture of 5 wt% Nafion solution and acetone (0.1 ml vol. mixture per mg of catalyst powder) for 30 min using an ultrasonic water bath. Then the catalyst slurry is coated onto carbon paper (Toray 90T) using a brush. The catalyst-coated carbon paper is dried in an oven for 30 min at 80 °C, and then hot pressed onto a nickel mesh at 80 °C and 10 kg cm^{-2} for 1 min. The composite electrode is then put in the oven and dried for another 30 min at 80 °C. PTFE tape is placed on the surface of the cathode in contact with air to prevent leakage of fuel–electrolyte solution. The fuel cell used a 0.3 M glucose in 1 M KOH solution as the fuel–electrolyte mixture operated at 30 °C.

3. Results and discussion

Fig. 1 shows the SEM and TEM images of MnO_2–C nanocomposite and Au/MnO_2–C catalyst. Needle like MnO_2 nanowires are observed from the SEM image in Fig. 1(a). Carbon nanoparticles are dispersed inside the MnO_2 nanowire structure forming a composite support. This is further demonstrated by the TEM image in Fig. 1(b). The diameter of the MnO_2 nanowires is approximately 10 nm as seen from Fig. 1(b). The TEM image of Au/MnO_2–C catalyst (Fig. 1(c)) shows that gold nanoparticles with diameters in the range of 4–8 nm are dispersed onto the MnO_2–C nanocomposite support. Fig. 1(d) shows the particle size distribution of Au nanoparticles on the MnO_2–C composite. The average particle size of Au nanoparticles is about 5.8 nm.

The crystal structure of the prepared MnO_2–C catalyst support and the Au/MnO_2–C catalyst are investigated using XRD and data are shown in Fig. 2. Both XRD patterns show a peak at about $2\theta = 26°$ which is associated with the carbon support (002).

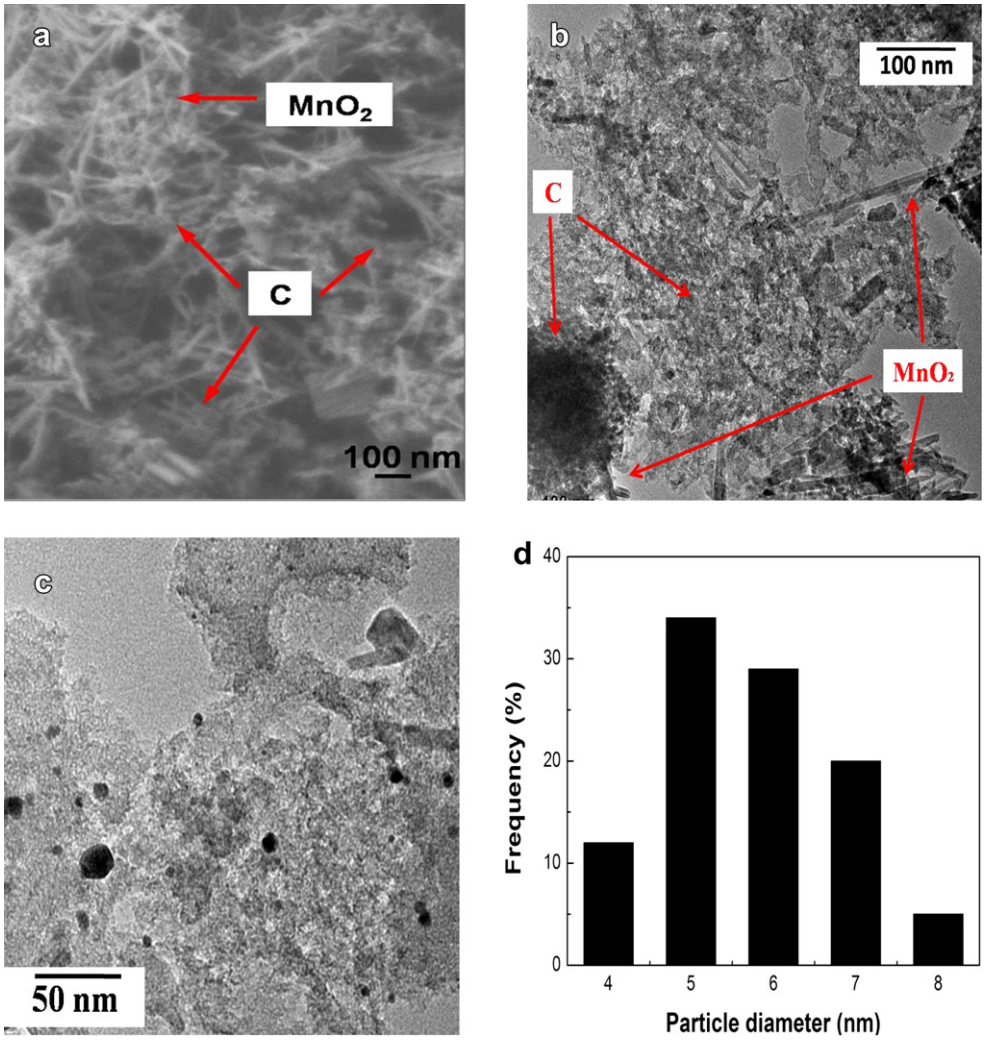

Fig. 1. (a) SEM micrograph of MnO_2/C, (b) TEM micrographs of MnO_2/C, (c) TEM of Au/MnO_2–C and (d) particle size distribution of Au/MnO_2–C.

Reflection peaks of MnO_2 at (220), (310), (400), (211), (301), (411), (600) indicate that the MnO_2 is present in the α-MnO_2 phase, with lattice constants of $a = 9.794$ Å, $c = 2.859$ Å; which are in agreement with the standard values (JCPDS 44-0141, $a = 9.784$ Å, $c = 2.863$ Å) [23]. The peaks of Au nanoparticles occur at 38.4° (111), 44.5° (200), 64.8° (220) and 77.6° (311), which also agree with the standard values [24]. These peaks suggest that Au nanoparticles have a face-centred cubic (fcc) structure [24]. The narrow peaks from the XRD scans indicate a crystallised structure of nanocomposite and catalyst. Using the Au(220) peak and the Debye–Scherrer equation, the Au nanoparticle is 5.6 nm in size [11], which is comparable with the results from TEM measurement.

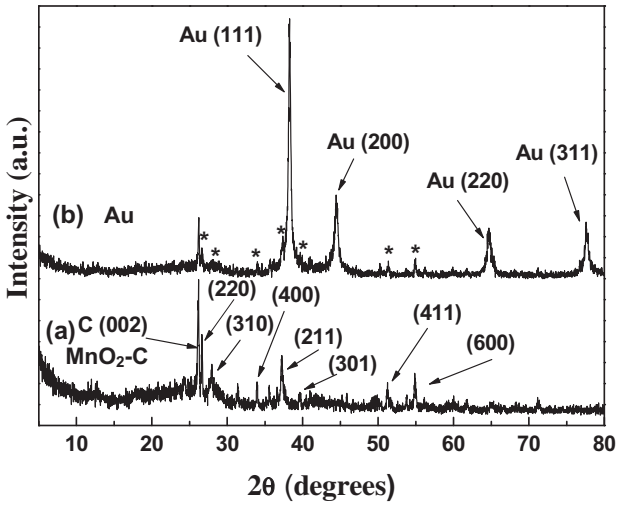

Fig. 2. XRD patterns of (a) MnO_2/C and (b) Au/MnO_2–C.

Electrocatalytic properties of MnO_2–C and Au/MnO_2–C for glucose oxidation are investigated in 0.5 M glucose and 1 M NaOH aqueous solution by cyclic voltammetry. Fig. 3(a) shows the CV of the MnO_2–C support in the absence and presence of 0.5 M glucose in 1 M NaOH solution. Without addition of glucose, there are a pair of redox peaks (P1) at −0.20 V (oxidation) and −0.48 V (reduction) which are related to the proton insertion process between MnO_2 and MnOOH [25]. In the presence of glucose, another oxidation peak (P2) is observed at around 0.14 V, which is probably caused by glucose oxidation. The catalytic effect of MnO_2 towards the oxidation of glucose is probably due to a parallel catalytic reaction [22,23]. With the presence of glucose, MnO_2 acts both as the catalyst support and a catalyst for glucose oxidation. As soon as MnO_2 is reduced to the lower valence state of MnOOH, by glucose, it is electro-oxidised back to MnO_2 on the electrode surface.

Fig. 3(b) compares the CVs of glucose oxidation performance for the prepared Au/MnO_2–C (20 wt%), commercial Pt/C (40 wt%,

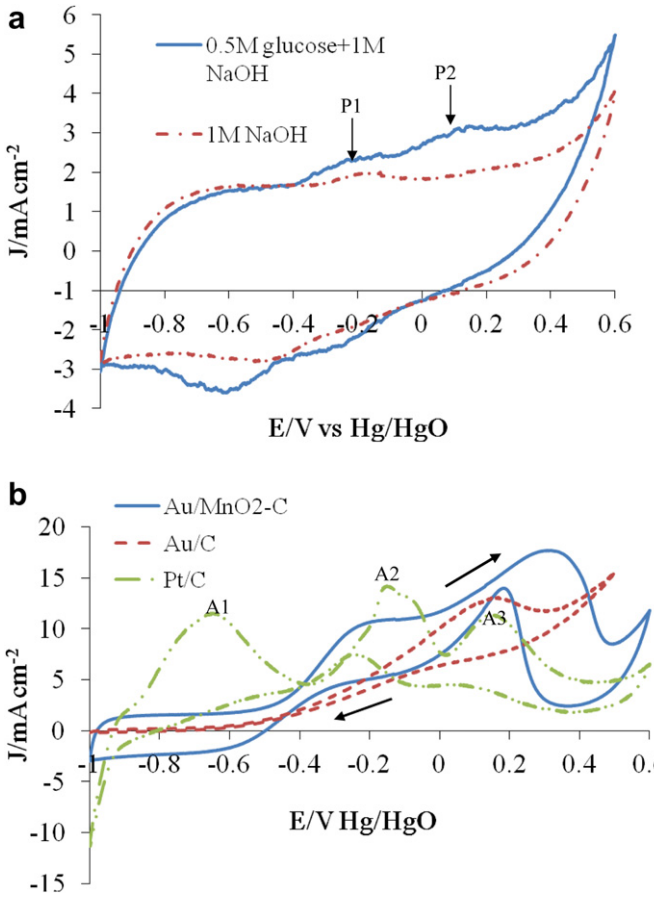

Fig. 3. Cyclic voltammograms of (a) MnO_2/C in the absence and presence of 0.5 M glucose in 1 M NaOH solution; (b) Au/MnO_2–C, commercial Au/C and Pt/C in the presence of 0.5 M glucose in 1 M NaOH solution. Scan rate: 50 mV s^{-1}, room temperature.

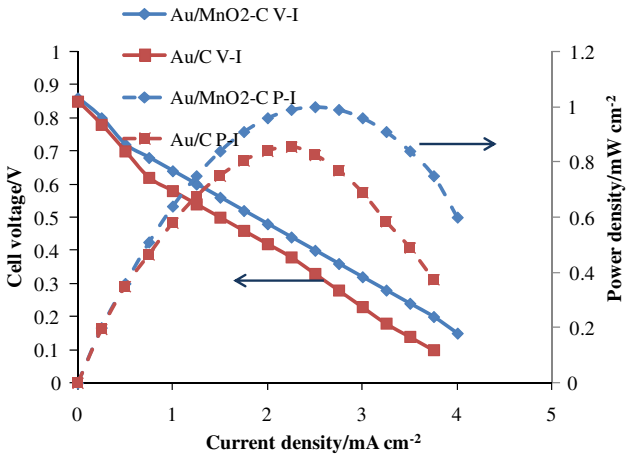

Fig. 4. Polarisation curves for fuel cells using 0.3 M glucose in 1 M KOH solution. Anode: Au/MnO_2–C (20 wt%) and Au/C (40 wt%) catalysts, cathode: activated charcoal, loading: 3 mg cm^{-2}, temperature: 30 °C.

Johnson Matthey) and Au/C (40 wt%, Arora Matthey) catalysts. The average particle size of the commercial Pt/C and Au/C catalysts was about 4 nm and 20 nm, respectively. Different shapes of the CVs are obtained. Three clear oxidation peaks A1, A2 and A3 are visible for glucose oxidation on Pt/C catalyst which are in agreement with the results in the literature [26]. The peak A1 is due to chemisorptions and dehydrogenation of glucose at low potentials. The A2 peak appeared at the OH^- adsorbed catalyst surface is a result of direct glucose oxidation from the bulk to gluconolactone, which is further hydrolysed to gluconate. The A3 peak is obtained on the already oxidised catalyst surface and may be caused by oxidation of adsorbed residues. With the Au/C catalyst, the main oxidation peak is found at 0.1–0.2 V. In the backward scan, an oxidation peak is observed for Au/C at −0.1–0 V, which is associated with reduction of the oxidative layer of gold, as described by Pasta et al. [13]. For Au/MnO_2–C, two strong oxidation peaks are observed at −0.3 to −0.2 V and 0.3–0.4 V, which are attributed to oxidation of MnOOH and glucose, respectively. An oxidation peak at 0.2 V in the backward scan is related to oxidation of un-oxidised glucose from the forward scan. Among the three catalysts studied, the highest glucose oxidation current is achieved by Au/MnO_2–C catalyst. As the gold component is 20 wt% in the Au/MnO_2–C catalyst, the actually gold loading is 0.6 mg cm^{-2} Au, only half that used in 40 wt % Pt/C and Au/C catalysts. This implies that with the nanocomposite substrate MnO_2–C, the amount of noble metal catalyst can be largely reduced yet achieving higher catalytic activity.

Fuel cell performance with Au/MnO_2–C and Au/C anode catalysts, and activated charcoal as cathode catalyst, are compared in Fig. 4. The open circuit voltages (OCVs) are similar for both systems: 0.86 V for Au/MnO_2–C and 0.85 V for commercial Au/C. The maximum power density of the fuel cell using Au/MnO_2–C catalyst is 1.1 mW cm^{-2} (specific mass activity of 1.8 mW cm^{-2} mg^{-1} Au) at a cell voltage of 0.4 V and a current density of 2.5 mA cm^{-2}, whereas that of the commercial Au/C catalyst is 0.86 mW cm^{-2} at 0.3 V, (specific mass activity of 0.72 mW cm^{-2} mg^{-1} Au). The specific mass activity of Au using the Au/MnO_2–C catalyst is almost twice that achieved with the commercial catalyst. The fuel cell performance is comparable to the performance reported on Pt/Au catalyst [11], but with a lower noble metal loading. The higher power output with the Au/MnO_2–C is obtained mainly due to a lower activation voltage loss in the kinetic region, i.e. from 0.86 V to 0.70 V, compared with that for the Au/C, i.e. 0.85 V–0.60 V. This behaviour agrees with the CV study; further proving that improved catalytic activity is achieved with the gold nanoparticles supported on the MnO_2–C nanocomposite. MnO_2 nanowire is a key factor for improving activity. In future studies optimising the MnO_2 structure and composition of MnO_2–carbon can be used to further enhance the catalytic activity and reduce the noble metal loading. The fuel cell power output may be enhanced by applying anion exchange membrane electrode system and more active cathode catalysts.

4. Conclusions

Au/MnO_2–carbon catalyst has been synthesised for direct glucose alkaline fuel cells. Improved electrochemical catalytic activity for glucose oxidation is achieved with gold nanoparticles supported on MnO_2–C nanocomposite. The improved activity is due to a parallel catalytic effect from MnO_2. The maximum power density of the fuel cell at 30 °C with a passive air cathode using Au/MnO_2–C catalyst is 1.1 mW cm^{-2}. This power density is higher than that of the commercial Au/C catalyst with half of the gold loading. MnO_2–C nanocomposite demonstrates a promising approach for reducing noble metal loading and improving the catalytic activity of gold catalyst for glucose oxidation. Further improvement of the catalyst activity can be achieved by optimising MnO_2 structure and composition of MnO_2–C nanocomposite.

Acknowledgements

LL thanks Newcastle University for a URC Visiting Fellowship. The authors thank Dr Senthil Kumar Sakkarapalayam Murugesan for preparing MnO_2–carbon nanocomposite.

References

[1] D. Basu, S. Basu, Electrochimica Acta 55 (2010) 5775–5779.
[2] N. Fujiwara, S.-i. Yamazaki, Z. Siroma, T. Ioroi, H. Senoh, K. Yasuda, Electrochemistry Communications 11 (2009) 390–392.
[3] S. Calabrese Barton, J. Gallaway, P. Atanassov, Chemical Reviews 104 (2004) 4867–4886.
[4] M. Guerra-Balcázar, D. Morales-Acosta, F. Castaneda, J. Ledesma-García, L.G. Arriaga, Electrochemistry Communications 12 (2010) 864–867.
[5] H. Liu, B.E. Logan, Environmental Science & Technology 38 (2004) 4040–4046.
[6] N. Mano, Chemical Communications (2008) 2221–2223.
[7] H. Sakai, T. Nakagawa, Y. Tokita, T. Hatazawa, T. Ikeda, S. Tsujimura, K. Kano, Energy & Environmental Science 2 (2009) 133–138.
[8] L. An, T.S. Zhao, S.Y. Shen, Q.X. Wu, R. Chen, Journal of Power Sources 196 (2011) 186–190.
[9] E.H. Yu, X. Wang, U. Krewer, L. Li, K. Scott, Energy & Environmental Science 5 (2012) 5668–5680.
[10] S. Kerzenmacher, J. Ducrée, R. Zengerle, F. von Stetten, Journal of Power Sources 182 (2008) 1–17.
[11] D. Basu, S. Basu, Electrochimica Acta 56 (2011) 6106–6113.
[12] H. Yin, C. Zhou, C. Xu, P. Liu, X. Xu, Y. Ding, Journal of Physical Chemistry C 112 (2008) 9673–9678.
[13] M. Pasta, R. Ruffo, E. Falletta, C. Mari, C. Pina, Gold Bulletin 43 (2010) 57–64.
[14] J.P. Spets, Y. Kiros, M.A. Kuosa, J. Rantanen, M.J. Lampinen, K. Saari, Electrochimica Acta 55 (2010) 7706–7709.
[15] D. Basu, S. Basu, International Journal of Hydrogen Energy 37 (2012) 4678–4684.
[16] F.M. Cuevas-Muñiz, M. Guerra-Balcázar, F. Castaneda, J. Ledesma-García, L.G. Arriaga, Journal of Power Sources 196 (2011) 5853–5857.
[17] C. Jin, I. Taniguchi, Materials Letters 61 (2007) 2365–2367.
[18] Z. Liu, L. Huang, L. Zhang, H. Ma, Y. Ding, Electrochimica Acta 54 (2009) 7286–7293.
[19] X. Yan, X. Ge, S. Cui, Nanoscale Research Letters 6 (2011) 313.
[20] D. Basu, S. Basu, International Journal of Hydrogen Energy 36 (2011) 14923–14929.
[21] J. Chen, W.-D. Zhang, J.-S. Ye, Electrochemistry Communications 10 (2008) 1268–1271.
[22] D. Das, P.K. Sen, K. Das, Journal of Electroanalytical Chemistry 611 (2007) 19–25.
[23] Y.J. Yang, S. Hu, Electrochimica Acta 55 (2010) 3471–3476.
[24] I.-S. Park, K.-S. Lee, J.-H. Choi, H.-Y. Park, Y.-E. Sung, Journal of Physical Chemistry C 111 (2007) 19126–19133.
[25] I. Roche, E. Chaînet, M. Chatenet, J. Vondrák, The Journal of Physical Chemistry C 111 (2006) 1434–1443.
[26] K.D. Popovic, A.V. Tripkovic, R.R. Adzic, Journal of Electroanalytical Chemistry 339 (1992) 227–245.